Macrophage SH3 domain-containing GRB2-like protein B1 is required for Rab7-mediated mitophagy in inflammation during sea water drowning acute lung injury

HONGJUAN NING[1*], JINGYU DENG[2*], YONGHENG GAO[1], WEI ZHANG[1], JIAN CHEN[1], XIAN GUO[1] and FAGUANG JIN[1]

[1]Department of Pulmonary and Critical Care Medicine, Tangdu Hospital, Fourth Military Medical University, Xi'an, Shaanxi 710038, P.R. China; [2]Department of Cardiology, Xijing Hospital, Fourth Military Medical University, Xi'an, Shaanxi 710032, P.R. China

Received November 18, 2025; Accepted February 24, 2026

DOI: 10.3892/ijmm.2026.5809

Abstract. Acute lung injury (ALI) accompanied by an inflammatory response is an important complication after drowning. Macrophage activation and polarization are implicated in the inflammatory process of lipopolysaccharide (LPS)-induced ALI (LPS-ALI), but little is known about drowning-induced ALI (drowning-ALI). SH3 domain-containing GRB2-like protein B1 (SH3GLB1) is a member of the endophilin family and has been shown to be involved in mitochondrial morphological changes and autophagy. However, its role in ALI remains unclear. Thus, the present study aimed to examine the effects of macrophages in drowning-ALI and to elucidate the underlying molecular mechanism involved. In the present study, single-cell RNA-sequencing indicated that the regulation of macrophages in drowning-ALI was similar to that in LPS-ALI by single-cell profiling of lung immune cells isolated from the lungs. Specifically, SH3GLB1 was highly expressed in macrophages of drowning-ALI mouse models and was related to inflammation. Furthermore, SH3GLB1 deletion ameliorated LPS-ALI or drowning-ALI. By contrast, the restoration of SH3GLB1 expression provoked LPS-ALI and drowning-ALI. Mechanistically, SH3GLB1 was shown to interact with Rab7 to contribute to mitophagy, which resulted in mitochondrial dysfunction. Overall, these findings indicated that SH3GLB1 is required for Rab7-mediated mitophagy in inflammation during ALI and could be a novel target for lung protection.

Correspondence to: Professor Faguang Jin, Department of Pulmonary and Critical Care Medicine, Tangdu Hospital, Fourth Military Medical University, 169 West Changle Road, Xi'an, Shaanxi 710038, P.R. China
E-mail: jinfag@fmmu.edu.cn

*Contributed equally

Key words: acute lung injury, macrophage, SH3 domain-containing GRB2-like protein B1, Rab7, mitophagy

Introduction

Sea water drowning is a crucial public safety problem and is the third leading cause of accidental fatality, claiming ~372,000 lives annually worldwide (1,2). In near-drowning patients, acute lung injury (ALI) or acute respiratory distress syndrome (ARDS) is one of the most common complications. ALI is a life-threatening clinical syndrome that occurs in critically ill patients because of an uncontrolled systemic inflammatory response. This response can either result from direct injury to the lung or from indirect injury in the setting of a systemic process following lipopolysaccharide (LPS) exposure or drowning (3,4). However, the mechanisms through which ALI is induced by drowning have not been well elucidated.

Severe inflammatory responses, when coupled with an excessive oxidative stress response, are considered to be the main causes of ALI (5,6). The onset of ALI is followed by a strong inflammatory response in lung tissue. Inflammatory cells such as alveolar macrophages (AMs) infiltrate lung tissue and produce inflammatory cytokines (7). Also, the abnormal production of reactive oxygen species (ROS) is considered to further worsen the onset and development of lung injury (8). Our previous studies indicated that endothelial semaphorin 7A promoted seawater aspiration-induced acute lung injury through plexin C1 and β1 integrin (9). It was also shown that seawater inhalation induced ALI ROS generation and the endoplasmic reticulum stress pathway (10). This suggested that severe inflammatory responses and ROS production exited in drowning-induced ALI (drowning-ALI). Innate immune cells located in the lung epithelium play an essential role by producing pro-inflammatory factors to eliminate pathogens and releasing anti-inflammatory factors to maintain lung homeostasis (11). Pulmonary macrophage is a critical cell of the pneumonic innate immune system in lung injury, suggesting that macrophages are activated and polarized in response to LPS-induced lung injury (12). However, the effect of macrophages in drowning-ALI is poorly understood.

SH3 domain-containing GRB2-like protein B1 (SH3GLB1) or Bax-interacting Factor 1 (Bif 1), is an Endophilin B protein. SH3GLB1 is expressed in most tissues, with high expression in the heart and skeletal muscle (13). Studies have reported that SH3GLB1 plays a key role in cancer (14,15), Parkinson's disease (16), Alzheimer's disease (17) and cerebral ischemic injury (18). However, whether SH3GLB1 is involved in maintaining normal cardiac function and myocardial I/R injury remains unclear. Furthermore, the molecular mechanism responsible for SH3GLB1 related cardiac regulation requires further investigation.

Therefore, the objectives of this study were to examine the effects of macrophages in drowning-ALI and to elucidate the underlying molecular mechanism involved.

Materials and methods

Animals. All animal procedures followed the eighth edition (2011) of the Guide for the Care and Use of Laboratory Animals (https://www.ncbi.nlm.nih.gov/books/NBK54050/) and were approved by the Fourth Military Medical University Animal Ethics Committee (approval no. 20250088). A total of 20 SH3GLB1-deficient mice on a C57BL/6J background and 20 of their wild-type littermates were produced by Shanghai Model Organisms Center. Animals were housed at 22±0.5˚C and 60±5% relative humidity under a 12-h light/dark cycle. Mice were allocated randomly and subsequent histological and functional analyses were performed by investigators unaware of genotype.

Drowning- and LPS-induced ALI (LPS-ALI) models. A total of 30 8-week-old pathogen-free, 15 male WT C57BL/6 mice or 15 SH3GLB1 KO mice (20-22 g) were housed at 22±0.5˚C and 60±5% relative humidity under a 12-h light/dark cycle. Then they were used to establish an LPS-induced ALI model (19). Living conditions were as in the previous section. In brief, mice are anesthetized with isoflurane using an induction concentration of 5% for 2-5 min until the animals lose consciousness. For maintenance, the concentration was kept at 2.5% for 2-3 min, depending on the duration of seawater perfusion. Then, 50 μl of 10 mg/kg LPS (cat. no. O55:B5; MilliporeSigma) was slowly dripped into the lungs from the air pipe to the distal end of the lung with a microinjector. To induce drowning-related ALI, a seawater solution matching East China Sea parameters (1,300 mmol/l osmolality; pH 8.2; SW 1.05; containing 6.518 g/l NaCl, 3.305 g/l $MgSO_4$, 2.447 g/l $MgCl_2$, 1.141 g/l $CaCl_2$, 0.725 g/l KCl, 0.202 g/l $NaHCO_3$, 0.083 g/l NaBr) was slowly instilled at 4 ml/kg into the distal airways via a microinjector inserted through the trachea (20). After 0.5, 1, 2 and 3 h of seawater inhalation, arterial blood from the right common carotid artery was collected for blood gas analysis. $PaO_2/FiO_2 \leq 300$ mmHg (40 kPa) indicated successful modelling.

Histopathological analysis. Paraffin sections of lungs (5 μg) were stained with hematoxylin-eosin (room temperature; 1 min) and evaluated independently by two pathologists unaware of group assignment. Injury was graded 0-3 (absent to severe) for interstitial/alveolar oedema, hemorrhage, septal thickening and inflammatory-cell infiltration (21).

Single-cell preparation and single-cell RNA-sequencing. Lungs were harvested and enzymatically dissociated with 0.4 mg/ml collagenase A plus 0.4 mg/ml DNase to yield single-cell suspensions; material from identical time points was pooled. After Fc-blockade (anti-CD16/32, Invitrogen; cat. no. MFCR00), cells were stained with anti-CD45 (BioLegend, Inc.; cat. no. 480027) and CD45+ leukocytes were purified by fluorescence-activated cell sorting for subsequent assays. Using the 10X Genomics Chromium platform (Shanghai OE Biotech Co., Ltd.), barcoded gel beads were loaded to saturation so that each gel bead-in-emulsion (GEMs) contained one cell and one bead. After lysis, poly-A RNA hybridized to the beads, which were then pooled for reverse transcription; every cDNA received a 5' UMI and a cell-specific barcode. Libraries were checked on a Bioanalyzer 2,100 with an Agilent high-sensitivity DNA chip and quantified by the Qubit HS DNA kit (Q33230; Thermo Fisher, Inc.) before 150-bp paired-end sequencing on a NovaSeq 6,000 (Illumina, Inc.). Reads were demultiplexed and aligned with Cell Ranger 4.0 (10X Genomics, Inc.) under default settings. Gene Ontology (GO) functional enrichment and Kyoto Encyclopedia of Genes and Genomes (KEGG) pathway enrichment analyses of differentially expressed genes were performed with ClusterProfiler (v4.2.0; Shanghai OE Biotech Co., Ltd.). The SRA data are accessible with the following link: https://www.ncbi.nlm.nih.gov/sra/PRJNA1416051.

Flow cytometry analysis. After harvesting, cells were resuspended in BD Pharmingen Stain Buffer (BD Biosciences; cat. no. 554656;) and incubated for 30 min at 4˚C with the following macrophage-focused panel: APC-F4/80 (cat. no. 123115; BioLegend, Inc.; 5 μl), Pacific Blue-Ly6G (cat. no. 127612; BioLegend, Inc.; 5 μl), FITC-CD11b (cat. no. 101205; BioLegend, Inc.; 5 μl) and PE-CD11c (cat. no. 117307; BioLegend, Inc.; 5 μl). Viability was assessed with DAPI plus BD Horizon Fixable Viability Stain 780 (cat. no. 565388; 1:1,000) and 510 (cat. no. 564406; 1:1,000). Following three washes in stain buffer, samples were acquired on an ImageStream Mark II (Luminex) and analyzed with IDEAS v6.2 (Cytek Biosciences, Inc.).

Transmission electron microscopy (TEM). Lung tissue was initially fixed overnight at 4˚C in 4% glutaraldehyde prepared in PBS, then post-fixed for 1 h with 1% osmium tetroxide. After dehydration the specimens were resin-embedded and sectioned at 80 nm. Ultrastructural images were recorded on a JEOL JEM-1230 transmission electron microscope (JEOL, Ltd.) operating at 80 kV and mitochondrial cross-sectional areas were measured with ImageJ 1.54p (National Institutes of Health).

Reverse transcription-quantitative (RT-q) PCR. RNA was extracted with TRIzol® (cat. no. 15596026; Thermo Fisher Scientific, Inc.). The purity of extracted RNA was evaluated using the 260/280 ratio, with values between 1.8 and 2.0 indicating good purity. The RNA concentration ranged from 500 to 1,000 ng/ml. After gDNA removal (PrimeScript RT kit; cat. no. RR047A; Takara Biotechnology Co., Ltd.), cDNA was synthesized and analyzed by SYBR-based qPCR (SYBR Premix Ex Taq II; cat. no. RR820L; Takara Biotechnology

Co., Ltd. Transcript levels were quantified by the $2^{-\Delta\Delta Cq}$ method relative to GAPDH (22). Primers (provided by Beijing Tsingke Biotech Co., Ltd.): SH3GLB1, F 5'-GTGTGAGCGGAGAGG CG-3', R 5'-TCTTCTGTGAACTGCACGGC-3'; GAPDH, F: 5'-GACATGCCGCCTGGAGAAAC-3'; R: 5'-AGCCCAGGA TGCCCTTTAGT-3'.

Western blot analysis. Lung samples and bone marrow-derived macrophages (BMDMs) were homogenized in RIPA buffer. Proteins were separated by SDS-PAGE, transferred onto PVDF membranes, blocked with 5% skimmed milk for 1 h and probed with primary antibodies overnight at 4˚C. Primary antibodies: GAPDH (1:1,000; cat. no. ab8245; Abcam), HSP90 (1:1,000; cat. no. 13171-1-AP, Proteintech Group, Inc.), SH3GLB1 (1:1,000; cat. no. sc-374146, Santa Cruz Biotechnology, Inc.), LC3 (1:1,000; cat. no. 12741T; CST Biological Reagents Co., Ltd.), P62 (1:1,000; cat. no. ab109012, Abcam), Rab7 (1:1,000; cat. no. A12308, ABclonal) and Parkin (1:1,000; cat. no. ab77924, Abcam). After washing with 1X TBST (containing 0.1% Tween-20), membranes were incubated with HRP-conjugated secondary antibodies (1:5,000, cat. no. 7074S/7076S; CST Biological Reagents Co., Ltd.) and bands were revealed using ECL-HRP substrate (cat. no. WBAVDCH01; MilliporeSigma) and quantified in Image Lab (Bio-Rad Laboratories, Inc.).

Isolation, culture and BMDM treatments. Primary mouse BMDMs were isolated from 6- to 11-week-old mice sacrificed under approved protocols (23). Bones (femur/tibia) were dissected aseptically, cleaned of soft tissue and epiphyses removed. Marrow cavities were rinsed with ice-cold DMEM (cat. no. 11995; Gibco; Thermo Fisher Scientific, Inc.) using a 1 ml syringe. The flushed cells were pelleted (300 x g, 5 min, room temperature), subjected to red-cell lysis and filtered through a 40 μm nylon mesh (Falcon; Corning Life Sciences) to obtain a single-cell suspension. To drive differentiation, these bone-marrow progenitors were maintained for 7 days at 37˚C in complete DMEM (10% FBS, 1% P/S) supplemented with 20 ng/ml mouse M-CSF (cat. no. 315-02-500; PeproTech, Inc.). Differentiation was confirmed by flow-cytometric detection of F4/80. For experiments, macrophages were exposed to 200 ng/ml LPS (cat. no. S7850; Selleck Chemicals) dissolved in 20% artificial seawater for 24 h.

Bronchoalveolar lavage fluid (BALF) collection. After sedating the mice, the airways were washed by inserting a 14-G catheter into the trachea and gently instilling and withdrawing 1 ml of PBS three times; the resulting BALF was harvested for subsequent analyses (24).

ELISA assay. Post-ALI, carotid blood was withdrawn and centrifuged (1,000 rpm; 10 min; 4˚C) to obtain serum that was kept at -80˚C. In parallel, BALF was harvested. Cytokine concentrations (TNF-α, IL-6, IL-1β; cat nos. RK04875, RK00008 and RK05253; ABclonal Biotech Co., Ltd.) in both fluids were quantified with commercial ELISA kits following the supplier's protocol.

Seahorse analysis. Mitochondrial oxygen consumption rate (OCR) was monitored on an XF24 Extracellular Flux Analyzer (Agilent Seahorse; Agilent Technologies, Inc.) (25). BMDMs were plated at $1.6x10^5$ cells per XF24 well, transfected with siRNA for 48 h and treated as indicated. OCR was then recorded using the Mito Stress Test with the following injector concentrations: oligomycin 0.6 μM, FCCP 0.75 μM, antimycin A 2 μM and rotenone 1 μM. Basal and maximal respiration were extracted with Seahorse Wave desktop software Wave Desktop v2.6.3.5 (Agilent Seahorse; Agilent Technologies, Inc.); ATP-linked respiration and spare respiratory capacity were calculated according to the kit's algorithm.

Mitochondrial ROS assay. Mitochondrial ROS were visualized with MitoSOX Red (cat. no. M36008; Invitrogen; Thermo Fisher Scientific, Inc.) per the supplier's instructions. Fluorescence images were captured on an FV3000 confocal microscope (Olympus Corporation) and quantified by ImageJ v1.54p (National Institutes of Health) (26) In brief, the fluorescence of exposed cells/fluorescence of control cells represented ROS production and the average fluorescence intensity was analyzed by ImageJ v1.54p (National Institutes of Health).

Mitochondrial membrane potential (Δψm) measurements. Δψm was evaluated with the JC-1 assay (Beyotime Biotechnology) (27). After 20 min of incubation at 37˚C, healthy mitochondria (JC-1 aggregates) emitted red light (570 nm), whereas depolarized mitochondria (JC-1 monomers) emitted green light (535 nm). Red/green fluorescence ratios were acquired on an FV3000 confocal microscope (Olympus Corporation) and used as a proxy for Δψm.

Coimmunoprecipitation (Co-IP). BMDMs were rinsed three times with ice-cold PBS and solubilized in IP buffer (25 mM Tris-HCl pH 7.4, 150 mM NaCl, 1% NP-40, 1 mM EDTA, 5% glycerol; cat. no. 87787; Thermo Fisher Scientific, Inc.) plus protease/phosphatase inhibitors (cat. no. 5872; CST Biological Reagents Co., Ltd.). Lysates were rotated overnight at 4˚C with 1 μg antibody, then with Protein A/G magnetic beads for 4 h. After three washes with IP buffer, bead-bound proteins were eluted, electrophoresed and transferred to PVDF for blotting with anti-SH3GLB1 and anti-Rab7. A total of 40 μl of original lysate were retained as input/loading control.

LC-MS/MS analysis. LC-MS/MS was contracted to Shanghai Baipu Biotechnology Co., Ltd. Gel slices were reduced, alkylated, acetone-precipitated and digested overnight with trypsin (Promega Corporation; 1:50 w/w) at 37˚C. Peptides were recovered by centrifugation (16,000 x g; 15 min; 20˚C), desalted on C18 StageTips and loaded onto a trap column in 0.1% FA. Separation used a 300 nl min^{-1} home-packed RP column coupled to a Q-Exactive HF-X (Thermo Fisher Scientific, Inc.). A Top-20 DDA method (350-1 800 m/z; 60,000 at 200 m/z for MS, 15,000 at 200 m/z for HCD-MS/MS) generated raw files searched against the UniProt mouse database with MaxQuant 1.6.1.0. Data are available via ProteomeXchange with identifier PXD073650 (https://www.ebi.ac.uk/pride/archive/projects/PXD073650).

Cell transfection and adenoviral infection. BMDMs were transfected with 20 nM siRNA (sense 5'-GCACAGUGU UACCAGUAUA, antisense 5'-UAUACUGGUAACACU

GUGC) using Lipofectamine® RNAiMAX (cat. no. 13778075; Invitrogen; Thermo Fisher Scientific, Inc.) for 6 h, then maintained in fresh complete medium for 48 h at 37˚C. For overexpression, cells were exposed to adenovirus (MOI 50) for 6 h, washed and cultured another 48 h at 37˚C; efficiency was verified by western blotting.

Immunofluorescence staining. To label mitochondria or lysosomes, live BMDMs infected with SH3GLB1-expressing adenoviral vectors were stained with the MitoTracker Red CMXRos probe (150 nM; cat. no. M7512; Thermo Fisher Scientific, Inc.) or LysoTracker Red DND99 probe (100 nM; cat. no. T39855; TargetMol Chemicals Inc.) at 37˚C for 20 min. The images were acquired with a confocal microscope (FV3000; Olympus Corporation).

Mitophagic flux analysis. A mitochondrion-targeting Keima (mKeima) adenovirus (Shanghai GeneChem Co., Ltd.) was used to infect the cells for 6 h. Their Keima fluorescence density was observed at 48 h after mKeima infection by a Zeiss LSM780 confocal microscope (Zeiss AG). Lysosomal mitochondrial degradation was evaluated with mKeima as a marker for the evaluation of mitophagic flux. The pH sensitivity of mKeima was used to determine if the mitochondria were in acidic (561 nm, red) or neutral compartments (excitation 488 nm, green). Pairs of images were collected in sequence at 488 nm (green) and 561 nm (red) wavelengths for ratiometric analysis of mKeima fluorescence (28). The fluorescence density of mKeima was calculated as the ratio of 561/488 nm fluorescence integrated densities in each x630 field by ImageJ v1.54p (National Institutes of Health).

Pull-down assays. Recombinant GST-tagged proteins were incubated with glutathione sepharose beads for 4 h at 4˚C. After pre-binding, the beads were incubated overnight at 4˚C with purified interacting proteins in binding buffer C (50 mM Tris pH 7.4, 150 mM NaCl, 1 mM EDTA, 6 mM sodium deoxycholate, 1% NP-40, 1 mM PMSF, plus protease inhibitors). Beads were washed extensively with the same buffer and bound proteins were eluted in 2X SDS sample buffer for immunoblot analysis.

Statistical analysis. Continuous variables are presented as the means ± Standard deviations. The normality of the data distribution was examined with a Shapiro-Wilk normality test. Two-tailed Student's t-tests and Mann-Whitney U tests were performed to see if there were any significant differences between the two groups. A one-way ANOVA was used to compare more than two variables with one independent variable, followed by a Tukey multi-comparison test. One-way ANOVA was used to evaluate the difference between time and concentration, followed by Dunnett's multi-comparison test. Data were analyzed using the GraphPad Prism Software 8.3.0 (Dotmatics) and SPSS Statistics, v25 (IBM Corp.). $P<0.05$ was considered to indicate a statistically significant difference.

Results

The regulation of macrophages in drowning-ALI is similar to that in LPS-ALI. The mice were treated with sea water, followed by hematoxylin and eosin staining. Compared with that in the normal group (sham), on the first day, lung inflammation was markedly aggravated, characterized by inflammation in the bronchi and alveoli, inflammatory cell infiltration, thickening of the alveolar septa and pulmonary oedema. From Day 1-3, the degree of lung inflammation gradually decreased, with inflammation limited to the peribronchial area. By Day 5, the inflammatory infiltration had recovered (inflammation moved into the repair phase) (Fig. 1A). Moreover, scoring of the lung injury revealed that the inflammation score was the highest on the first day (Fig. 1B).

To dissect the contribution of immune cells to drowning-ALI progression, we performed single-cell profiling. Lungs were collected from sham mice and mice after sea water administration for 1, 3 and 5 days. Then, the lung cells were normalized and clustered and the clusters were annotated on the basis of their specific gene expression markers: macrophages ($CD68^+C5ar1^+$), dendritic cells ($CD11c^+MHC\text{-}II^+Dpp4^+$), T and natural killer T (NKT) cells ($CD3e^+$), B cells ($CD19^+CD79a/b^+$), neutrophils ($CXCR2^+C5ar1^+$) and NK cells ($NKg7^+NCR1^+Gzma^+$; Fig. 1C). It was found that on the first day of seawater treatment, the macrophages in the lung tissue were depleted and the proportion of neutrophils increased. On the third day, the number of neutrophils began to decrease and the proportion of macrophages increased. On the fifth day, the neutrophils were depleted and the proportion of macrophages increased (Fig. 1D and E). Although macrophages are implicated in the inflammatory process of ALI, little is known about their role in drowning-ALI. To determine the regulation of macrophages in drowning-ALI, the macrophages were classified and it was found that, on the first day of seawater treatment, the alveolar macrophages were depleted. On the third day, both alveolar macrophages and mononuclear macrophages began to increase in number. On the fifth day, the number of alveolar macrophages increased (Fig. 1F-H). Alveolar macrophages mostly originate from mononuclear macrophages in ALI. Thus, single-cell sequencing trajectory analysis was performed and it was found that after administration to sea water, alveolar macrophages were derived mainly from mononuclear macrophages, which was consistent with the source of alveolar macrophages in ALI (Fig. 1I). Thus, to verify the pattern of macrophages in seawater-induced acute lung injury, flow cytometry analysis of F4/80 (marked macrophages) and Ly6G (marked neutrophils) was conducted. The results revealed that on Day 1 after seawater treatment, the macrophages were depleted, whereas the number of neutrophils sharply increased. On Days 3 and 5, the number of macrophages increased, whereas the number of neutrophils decreased. Furthermore, flow cytometry antibodies against CD11c were used to identify alveolar macrophages and antibodies against CD11b were used to identify monocyte-derived macrophages. $CD11c^+$ cells were markedly reduced on Day 1 after seawater treatment and gradually increased on Days 3 and 5. This finding indicates that on Day 1 after seawater treatment, the alveolar macrophages were depleted but increased on Days 3 and 5 and mostly differentiated from monocyte-derived macrophages (Fig. 1J), which was consistent with the single-cell sequencing data. These data indicate that immune cells, particularly macrophages, in drowning-ALI were similar to those involved in LPS-induced ALI.

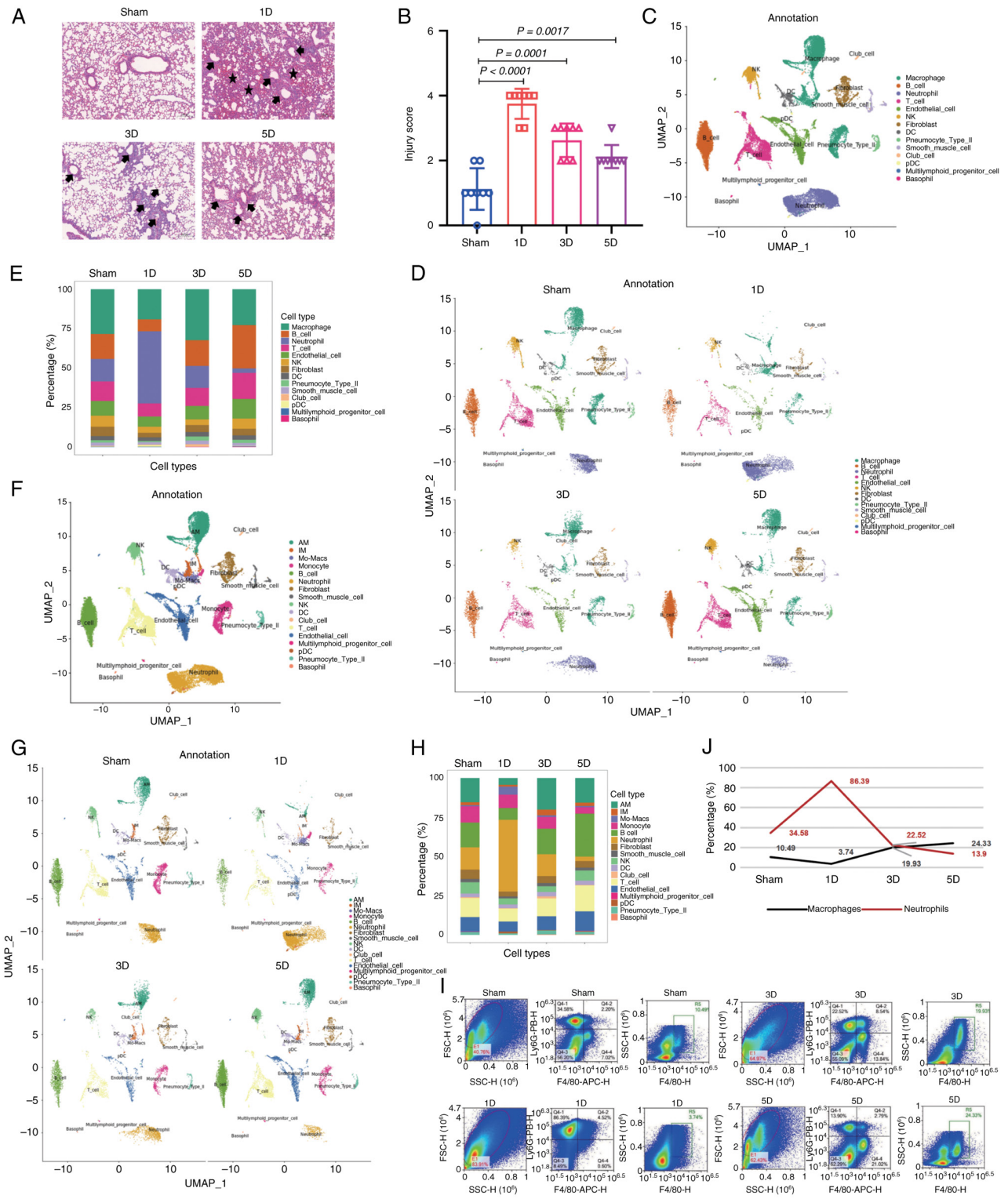

Figure 1. The regulation of macrophages in drowning-ALI was similar to that in LPS-ALI. (A) Lung tissues were histologically investigated by hematoxylin and eosin staining (scale bars, 200 μm). (B) Representative severity scores of lung injury (n=8). (C and D) UMAP analysis of immune cells in the lungs of sham- and sea water-treated mice; the colored unsupervised clustering results with cell type annotations are shown on the right. (E) Proportions of different cells in the lungs of the sham and sea water groups. (F and G) UMAP analysis of macrophages in the lungs of sham- and sea water-treated mice; the colored unsupervised clustering results with cell type annotations are shown on the right. (H) UMAP plots depicting the projection of macrophages from various stages of ALI on a 2D map. (I) Representative flow cytometry analysis of Ly6G and CD11c from F4/80$^+$ cells in the lung. (J) Representative analysis of the regulation of macrophages and neutrophils in sea water-induced ALI. The data are presented as the means ± SEMs. P<0.05 was considered to indicate a statistically significant difference. ALI, acute lung injury; LPS, lipopolysaccharide; UMAP, uniform manifold approximation and projection.

The mitochondrial protein SH3GLB1 is highly expressed in alveolar macrophages in drowning-ALI. Mitochondria play essential roles in macrophage inflammation during LPS-ALI. Transmission electron microscopy revealed that sea water induced mitochondrial morphological abnormalities, as indicated by greater swelling, a decreased number of

mitochondrial cristae and a reduced area of cristae (Fig. 2A). Next, single-cell sequencing data was analyzed and the top 15 mitochondrial proteins identified, among which SH3GLB1 had the highest score (Fig. 2B). Furthermore, it was found that SH3GLB1 was highly expressed in alveolar macrophages and that its expression was highest on the third day of seawater treatment (Fig. 2C). On the basis of the expression of SH3GLB1, the present study subsequently distinguished between alveolar macrophages with high and low expression of SH3GLB1 (Fig. 2D and E). It was found that the alveolar macrophages with high SH3GLB1 expression were depleted on the first day of seawater treatment, increased on the third day and increased on the fifth day. This finding was consistent with the changes in macrophages. To determine the effect of sea water on SH3GLB1, western blotting and qPCR was used to assess its expression. SH3GLB1 expression was elevated in alveolar macrophages treated with seawater (Fig. 2F and G). These results indicated a strong association between increased SH3GLB1 expression and sea water-induced ALI.

SH3GLB1 deficiency protected against inflammation in ALI. The present study subsequently performed Gene Ontology (GO) and Kyoto Encyclopedia of Genes and Genomes (KEGG) pathway enrichment analyses based on SH3GLB1 expression. The results indicated that SH3GLB1^{high} AMs showed an enrichment in regulation of the inflammatory response and the oxidative stress response (Fig. 3A-C). To assess the effects of SH3GLB1 on ALI, SH3GLB1 KO mice were generated. To gain insight into the function of increased SH3GLB1 in ALI, SH3GLB1 KO and control WT mice were subjected to sea water treatment or a sham operation at 8 weeks of age. Notably, SH3GLB1 deficiency markedly improved sea water-induced ALI and LPS-ALI (Fig. 3D and E). The present study next measured the concentration of inflammatory factors in the BALF via ELISA and found that SH3GLB1 deficiency markedly decreased the sea water- or LPS-induced expression of inflammatory factors, including IL-1β, TNFα and IL-6 (Fig. 3F-H). In agreement with these results, SH3GLB1 deficiency reduced the sea water- or LPS-induced elevations in the serum concentrations of these inflammatory factors (Fig. 3I-K). To determine whether SH3GLB1 defects directly influence macrophage inflammation, we isolated BMDMs and then infected them with adenoviruses carrying siRNA targeting SH3GLB1 or a control scrambled siRNA. Western blot and qPCR analyses revealed that the siRNA effectively knocked down SH3GLB1 expression (Fig. 3L-M). As expected, ELISA analysis demonstrated that SH3GLB1 knockdown in BMDMs markedly reduced the secretion of inflammatory factors induced by LPS (Fig. 3N) and sea water (Fig. 3O). Taken together, the data indicated that SH3GLB1 defects were critical for protection against ALI.

Reduced SH3GLB1 ameliorates mitochondrial dysfunction in macrophages from ALI model mice. There is a close relationship between ALI and mitochondrial homeostasis. Next, the present study examined the mitochondrial morphology of SH3GLB1 KO and WT mice at 8 weeks old by means of TEM. At 8 weeks old, no significant changes in mitochondrial morphology were seen in the SH3GLB1 KO mice compared with the control WT. However, it was found that SH3GLB1 KO alleviated mitochondrial morphological abnormalities, as indicated by greater swelling, a decreased number of mitochondrial cristae and a reduced area of cristae induced by sea water (Fig. 4A).

Given that SH3GLB1 deficiency improved BMDM inflammation, it was next determined whether SH3GLB1 can directly affect mitochondrial function in BMDMs. Therefore, the mitochondrial membrane potential was tested using JC-1 staining and it was found that SH3GLB1 knockdown markedly increased the mitochondrial membrane potential in BMDMs under LPS conditions (Fig. 4B and C). Additionally, confocal microscopy images to were used assess mitochondrial ROS levels and it was found that SH3GLB1 knockdown decreased mitochondrial ROS production in BMDMs under LPS conditions (Fig. 4D). Due to these profound alterations in the structure of mitochondria and mitochondrial oxidation, OCR was analyzed to assess mitochondrial respiration. As expected, SH3GLB1 knockdown markedly enhanced mitochondrial respiration in BMDMs under LPS, as shown by basal respiration, ATP production, maximum respiration and reserve respiration (Fig. 4E). Taken together, these data showed that the inactivation of SH3GLB1 increases the potential loss of mitochondrial membrane potential, reduces the generation of mitochondrial ROS and induced by LPS in mitochondrial respiratory failure.

Restoration of SH3GLB1 expression provokes ALI and mitochondrial dysfunction. To determine whether SH3GLB1 overexpression can aggravate sea water-induced ALI or LPS-ALI, SH3GLB1 expression was restored by inhalation of adenoviruses expressing the SH3GLB1-GFP fusion protein into the mouse lung. Notably, the hematoxylin and eosin results indicated that SH3GLB1 overexpression markedly aggravated sea water-induced ALI or LPS-ALI (Fig. 5A and B). Furthermore, the present study measured the concentrations of inflammatory factors in the BALF and found that SH3GLB1 overexpression markedly increased the sea water- or LPS-induced expression of inflammatory factors (Fig. 5C and E). Similarly, SH3GLB1 overexpression increased sea water or LPS-induced increases in the serum concentrations of these inflammatory factors (Fig. 5F-H). Next, SH3GLB1 was overexpressed in BMDMs via adenovirus infection. Western blot and qPCR analyses revealed markedly increased expression of SH3GLB1 in BMDMs (Fig. 5I and J). ELISAs revealed that SH3GLB1 overexpression in BMDMs markedly promoted the secretion of inflammatory factors induced by LPS (Fig. 5K) and sea water (Fig. 5L). Overall, the data revealed that restoring SH3GLB1 expression in the lung exacerbated ALI.

Next, alveolar macrophages (AMs) mitochondrial morphology was examined using TEM in SH3GLB1-overexpressing and control mice at 8 weeks of age. No significant alterations in mitochondrial morphology were observed in SH3GLB1-overexpressing mice compared with control mice. However, SH3GLB1 overexpression provoked mitochondrial morphological abnormalities, as indicated by increased swelling, an increased number of mitochondrial cristae and an increased area of cristae induced by sea water or LPS (Fig. 6A). The present study also found that SH3GLB1 expression markedly decreased the mitochondrial membrane

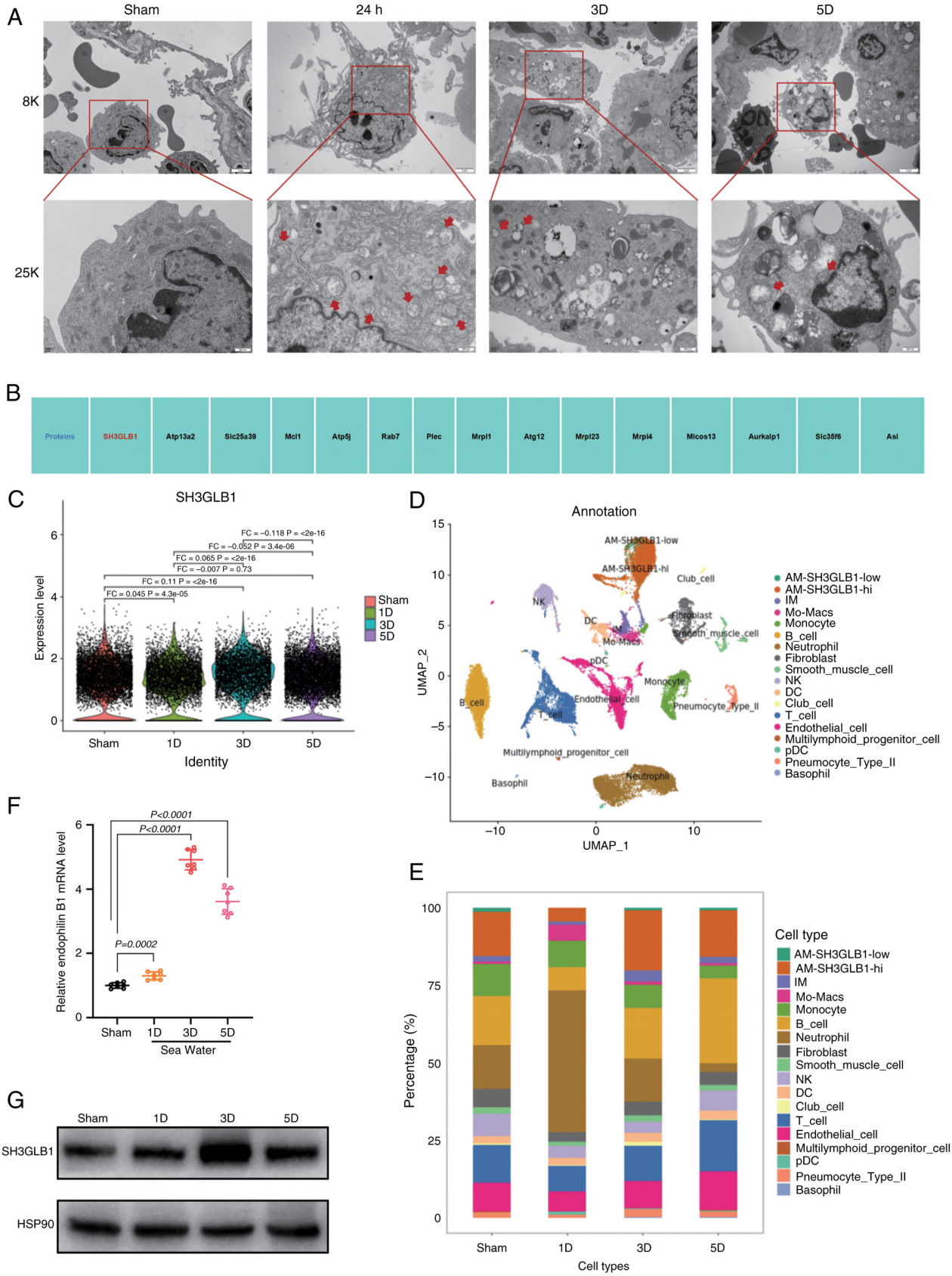

Figure 2. The mitochondrial protein SH3GLB1 was highly expressed in alveolar macrophages in drowning-ALI. (A) Representative TEM images of AM mitochondria in the lung (the red arrow indicates injured and swollen mitochondria; scale bars, 2 μm/500 nm). (B) Representative analysis of single-cell sequencing data and identification of the top 15 mitochondrial proteins. (C) Representative macrophage subcluster-specific expression patterns of SH3GLB1 between the sham and sea water groups. (D) UMAP analysis and (E) percentages of high and low SH3GLB1 expression in AMs treated with sham or sea water; colored unsupervised clustering results with cell type annotations are shown on the right. (F) Relative SH3GLB1 mRNA levels in alveolar macrophages from sham- or sea water-induced ALI model mice (n=7). (G) Representative western blots of SH3GLB1 protein levels in sham- or sea water-induced ALI model mice. The data are presented as the means ± SEMs; P<0.05 was considered to indicate statistical significance. SH3GLB1, SH3 domain-containing GRB2-like protein B1; ALI, acute lung injury; UMAP, uniform manifold approximation and projection; TEM, transmission electron microscopy; AMs, alveolar macrophages.

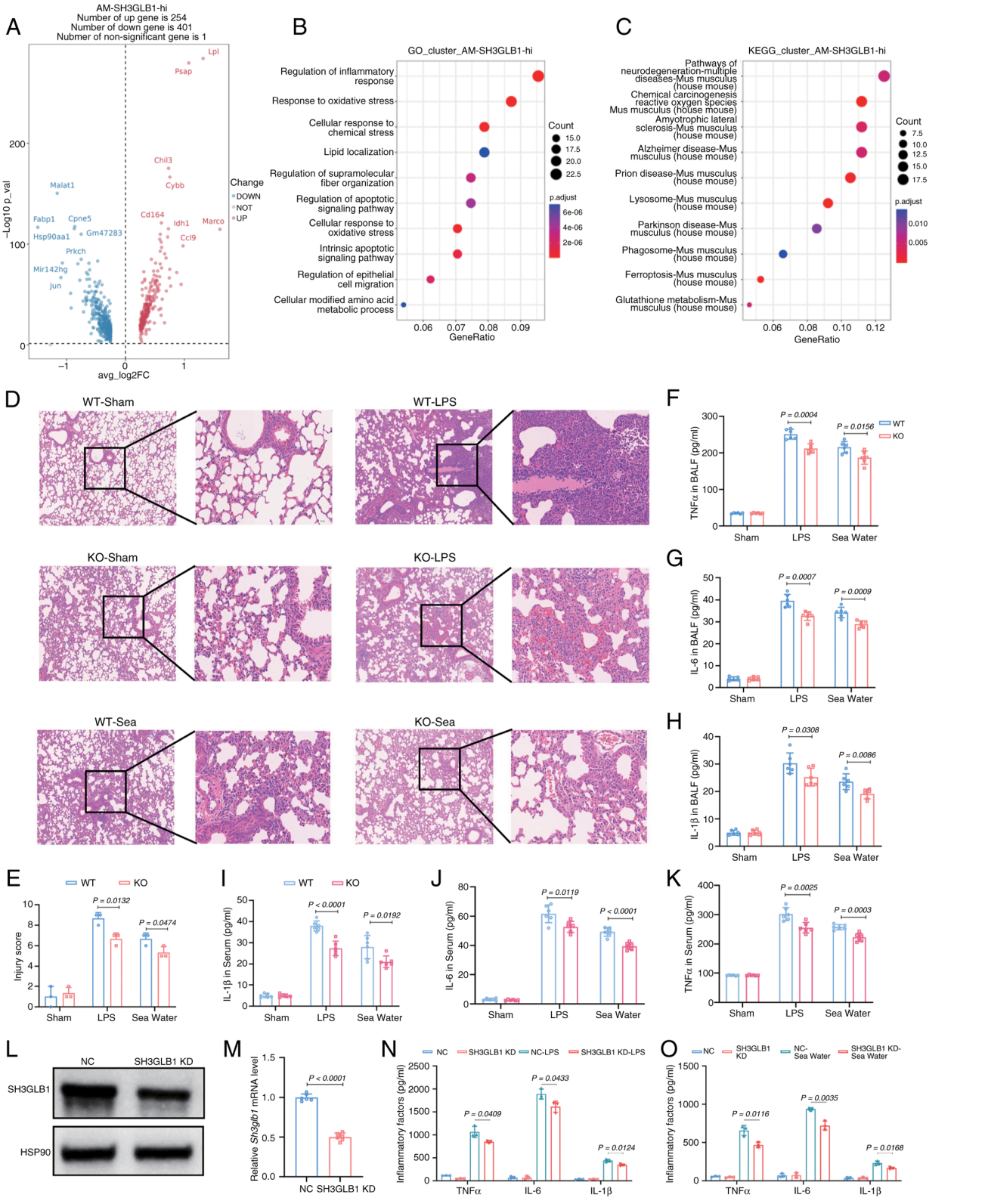

Figure 3. SH3GLB1 deficiency protects against inflammation in ALI. (A) Gene expression of SH3GLB1^{high} AMs in cohort 1 (n=3) represented in a volcano plot, with the fold change (log2) expressed as the level in sham versus sea water-ALI subjects on the x-axis and the P-value on the y-axis (log10). Significantly (P<0.05) regulated genes are marked in colors: red indicates upregulated genes and blue indicates downregulated genes in ALI. (B) Representative GO analysis of SH3GLB1^{high} AMs. (C) Representative KEGG analysis of SH3GLB1^{high} AMs. (D) Representative hematoxylin and eosin staining of lung tissues (scale bars, 200 μm). (E) Representative severity scores of lung injury (n=3). Representative ELISA results showing the levels of inflammatory factors, including (F) TNFα, (G) IL-6 and (H) IL-1β, in the BALF (n=6). (I-K) Representative ELISA analysis of the levels of inflammatory factors, including (I) IL-1β, (J) IL-6 and (K) TNFα, in the serum (n=6). (L) Representative western blots of SH3GLB1 protein levels in NC or SH3GLB1-KD BMDMs. (M) Relative SH3GLB1 mRNA levels in (NC or SH3GLB1-KD BMDMs. n=6/group. Representative ELISA analysis of the levels of inflammatory factors, including IL-1β, IL-6 and TNFα, in the supernatants of cells treated with (N) LPS or (O) seawater, (n=3).The data are presented as the means ± SEMs; P<0.05 was considered to indicate statistical significance. SH3GLB1, SH3 domain-containing GRB2-like protein B1; AMs, alveolar macrophages, ALI, acute lung injury; GO, Gene Ontology; KEGG, Kyoto Encyclopedia of Genes and Genomes; BALF, bronchoalveolar lavage fluid; BMDMs, bone marrow-derived macrophages; KD, knockdown; WT, wild-type; KO, knockout; NC, negative control; LPS, lipopolysaccharide.

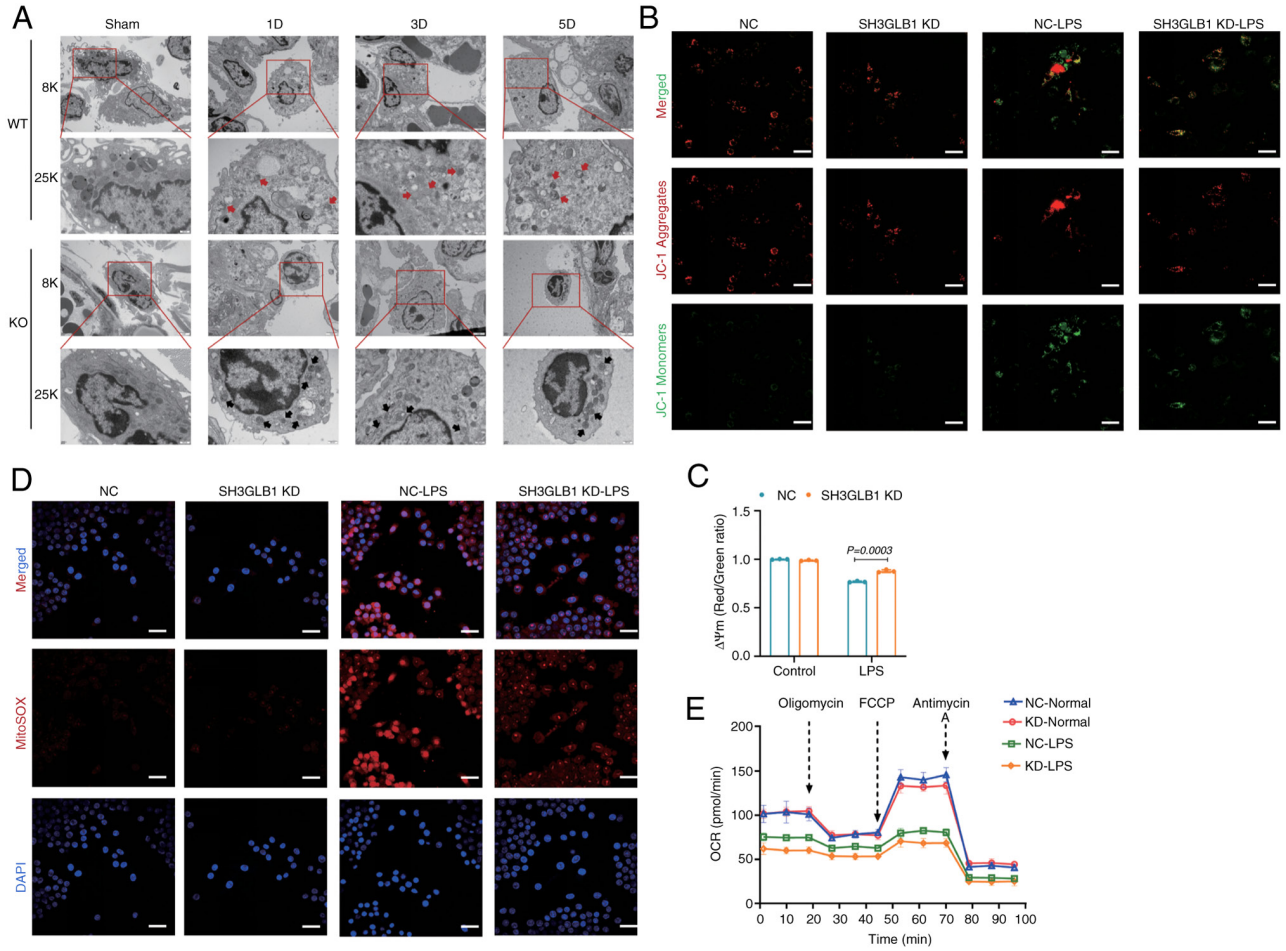

Figure 4. Reduced SH3GLB1 ameliorates LPS-induced mitochondrial dysfunction in macrophages. (A) Representative TEM images of macrophage mitochondria in the lung (scale bars, 2 μm/500 nm). Representative (B) confocal microscopy and (C) flow cytometry analysis of the mitochondrial membrane potential by JC-1 staining in BMDMs. A high level of green fluorescence (x-axis) represents a reduced mitochondrial membrane potential ($\Delta\Psi$m) and a high level of red fluorescence (y-axis) represents a normal $\Delta\Psi$m. The red fluorescence rate was analyzed (n=3). (D) Representative confocal microscopy images of mitochondrial ROS production (MitoSOX fluorescence; red) in NC or SH3GLB1-KD BMDMs under normal or LPS conditions (scale bar, 50 μm). (E) Analysis of the OCR of mitochondrial respiratory capacity, including basal respiration, ATP production, maximal respiration and spare respiration, in NC or SH3GLB1-KD BMDMs under normal or LPS conditions. The data are presented as the means ± SEMs; P<0.05 was considered to indicate statistical significance. SH3GLB1, SH3 domain-containing GRB2-like protein B1; LPS, lipopolysaccharide; TEM, transmission electron microscopy; BMDMs, bone marrow-derived macrophages; KD, knockdown; OCR, oxygen consumption rate; NC, negative control.

potential in BMDMs under LPS conditions (Fig. 6B and C). Additionally, confocal microscopy images indicated that SH3GLB1 overexpression increased mitochondrial ROS production in BMDMs under LPS conditions (Fig. 6D). The present study analyzed the mitochondrial OCR to assess the mitochondrial respiratory capacity. SH3GLB1 overexpression markedly reduced mitochondrial respiratory capacity, as indicated by basal respiration, ATP production, maximal respiration and spare respiration, in BMDMs under LPS conditions (Fig. 6E). Taken together, these data demonstrated that SH3GLB1 overexpression facilitated mitochondrial membrane potential loss and increased mitochondrial ROS production and mitochondrial respiratory dysfunction induced by LPS.

SH3GLB1 interacts with the lysosomal protein Rab7 to contribute to macrophage inflammation. To understand the molecular mechanisms of SH3GLB1 in macrophage function, IP-LC-MS/MS was employed to identify potential endogenous SH3GLB1 binding partners with a specific antibody against SH3GLB1 in BMDMs. The top 5 mitochondrial proteins were identified, among which Rab7 had the highest score (Fig. 7A). LPS or sea water increased Rab7 expression in BMDMs (Fig. 7B). Co-IP assays revealed that SH3GLB1 interacted with the lysosomal protein Rab7 (Fig. 7C). Moreover, immunofluorescence staining of BMDMs was performed and the colocalization of SH3GLB1 and Rab7 was observed (Fig. 7D). The present study subsequently conducted molecular docking analysis, which revealed a docking score of -289.57, which is less than -1 and the confidence score was 0.94 (a score higher than 0.7 indicated that Rab7 was more likely to bind to SH3GLB1) (Fig. 7E). The results of the pull-down experiments indicated that the purified Rab7 interacted with SH3GLB1 *in vitro* (Fig. 7F). These results suggested the direct binding between SH3GLB1 and Rab7. To determine whether SH3GLB1 promotes inflammation through Rab7, BMDMs were subjected to Rab7 overexpression or SH3GLB1 knockdown. The results revealed that the overexpression of Rab7 followed by the knockdown of SH3GLB1 failed to improve

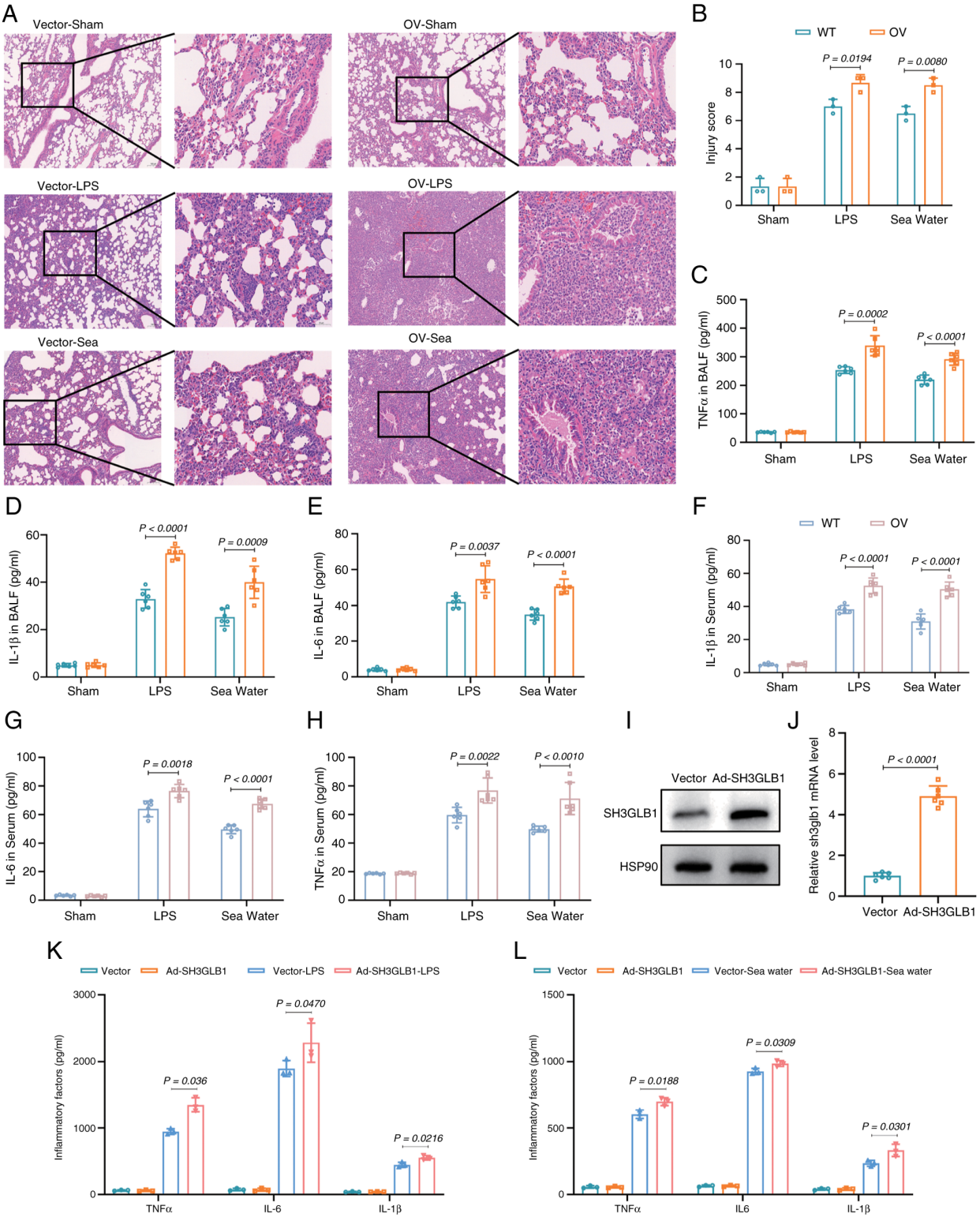

Figure 5. Restoration of SH3GLB1 expression provokes ALI. (A) Representative hematoxylin and eosin staining of lung tissues (scale bars, 100 μm). (B) Representative severity scores of lung injury (n=3). Representative ELISA results showing the levels of inflammatory factors, including (C) TNFα, (D) IL-1β and (E) IL-6, in the BALF (n=6). Representative ELISA analysis of the levels of inflammatory factors, including (F) IL-1β, (G) IL-6 and (H) TNFα, in the serum (n=6). (I) Western blots of SH3GLB1 expression. (J) Relative SH3GLB1 mRNA levels in vector- or SH3GLB1-overexpressing BMDMs. n=6/group. Representative ELISA analysis of the levels of inflammatory factors, including IL-1β, IL-6 and TNFα, in the supernatants of cells treated with (K) LPS or (L) sea water (n=3).The data are presented as the means ± SEMs; P<0.05 was considered to indicate statistical significance. SH3GLB1, SH3 domain-containing GRB2-like protein B1; ALI, acute lung injury; BMDMs, bone marrow-derived macrophages; WT, wild-type; OV; overexpression.

the release of inflammatory factors in BMDMs induced by LPS or sea water (Fig. 7G and I). Similarly, Rab7 knockdown followed by SH3GLB1 overexpression failed to change the release of inflammatory factors induced by LPS or sea water (Fig. 7H and J). These findings indicated that SH3GLB1 was required for Rab7 to contribute to macrophage inflammation.

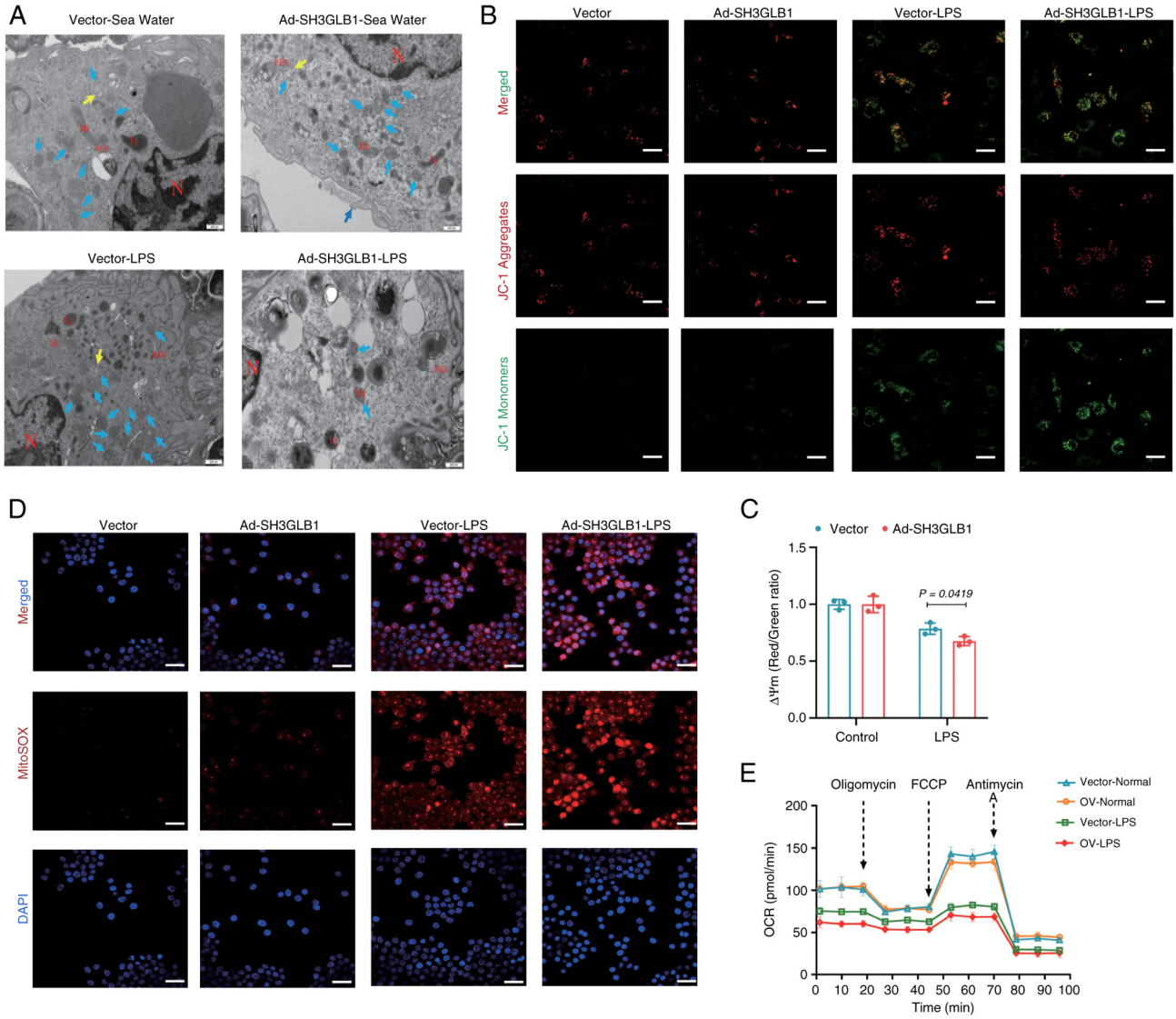

Figure 6. SH3GLB1 overexpression provoked mitochondrial dysfunction in macrophages. (A) Representative TEM images of macrophage mitochondria in the lung (scale bars, 2 μm/500 nm). Representative (B) confocal microscopy and (C) flow cytometry analysis of the mitochondrial membrane potential by JC-1 staining in BMDMs (n=3). (D) Representative confocal microscopy images of mitochondrial ROS production in vector- or SH3GLB1-OV BMDMs under normal or LPS conditions (scale bar, 50 μm). (E) Analysis of the OCR of mitochondrial respiratory capacity, including basal respiration, ATP production, maximal respiration and spare respiration, in vector- or SH3GLB1-overexpressing BMDMs under normal or LPS conditions. The data are presented as the means ± SEMs; P<0.05 was considered to indicate statistical significance. SH3GLB1, SH3 domain-containing GRB2-like protein B1; TEM, transmission electron microscopy; OCR, oxygen consumption rate; BMDMs, bone marrow-derived macrophages.

SH3GLB1 facilitates Rab7-mediated mitophagy. To clarify the localization of SH3GLB1 in BMDMs, immunofluorescence staining was performed and the colocalization of SH3GLB1 with lysosomes (labelled with LysoTracker) and mitochondria (labelled with MitoTracker) was observed (Fig. 8A). Rab7 plays a crucial role in the interaction between mitochondria and lysosomes, participating in the formation and fusion of mitochondrial autophagosomes, as well as in the contact and dissociation processes between mitochondria and lysosomes. To investigate whether SH3GLB1 is involved in Rab7-mediated mitophagy, cells overexpressing SH3GLB1 were treated with the mitochondrial autophagy inducer carbonyl cyanide-chlorophenylhydrazone and the overexpression of SH3GLB1 markedly increased the expression of the mitophagy-related proteins Parkin and LC3 while decreasing the expression of P62 (Fig. 8B-E). Additionally, mKeima expressed in BMDMs was imaged by confocal microscopy and assayed by flow cytometry. As shown in Fig. 8J and L, the overexpression of SH3GLB1 markedly facilitated mitophagy. However, SH3GLB1 knockdown decreased the expression of the mitophagy-related proteins Parkin and LC3 while decreasing the expression of P62 (Fig. 8F-I). Taken together, these findings indicated that SH3GLB1 facilitated adverse Rab7-mediated mitophagy.

Discussion

The present study demonstrated that the regulation of macrophages in drowning-ALI was similar to that in LPS-ALI. Specifically, SH3GLB1 was highly expressed in macrophages of drowning-ALI and was related to inflammation. Furthermore, SH3GLB1 deletion ameliorated LPS- or drowning-ALI. By

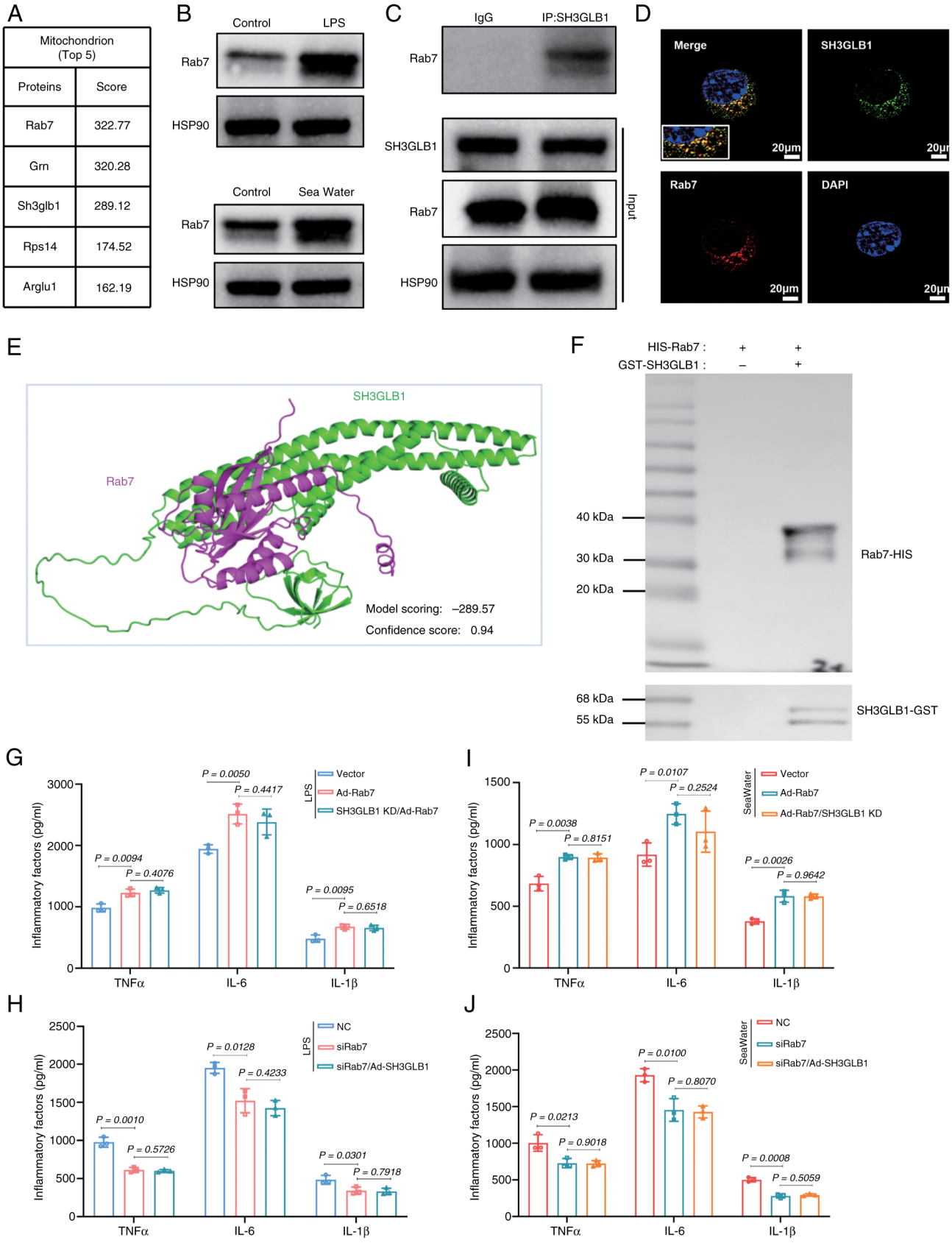

Figure 7. SH3GLB1 interacts with the lysosomal protein Rab7 to contribute to macrophage inflammation. (A) Representative top five proteins potentially binding to SH3GLB1 in mitochondria identified by mass spectrometry analysis. (B) Representative western blots of Rab7 protein levels in BMDMs treated with LPS or sea water. (C) Co-IP assay showing the interaction of SH3GLB1 with Rab7. (D) Representative images of immunofluorescence staining for SH3GLB1 (green) and Rab7 (red) in BMDMs. Scale bar, 20 μm. (E) Representative molecular docking analysis of SH3GLB1 and Rab7. (F) Western blots of recombinant Rab7 binding to recombinant SH3GLB1. Representative ELISA results showing the levels of inflammatory factors, including IL-1β, IL-6 and TNFα, in the supernatants of cells treated with (G and H) LPS (n=3) or (I and J) sea water (n=3). The data are presented as the means ± SEMs; P<0.05 was considered to indicate statistical significance. SH3GLB1, SH3 domain-containing GRB2-like protein B1; BMDMs, bone marrow-derived macrophages; LPS, lipopolysaccharide; Co-IP, coimmunoprecipitation.

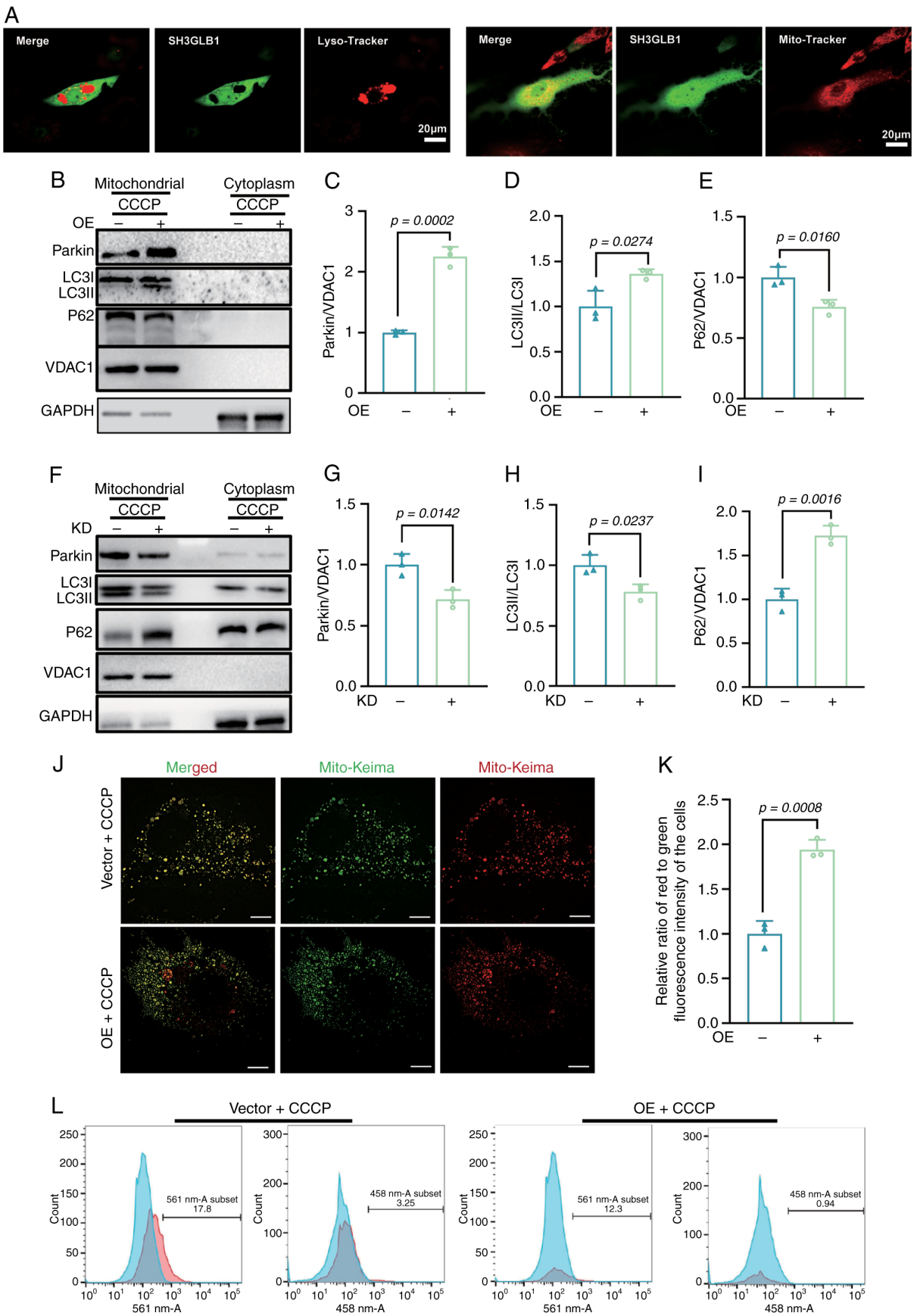

Figure 8. SH3GLB1 facilitated adverse Rab7-mediated mitophagy. (A) Representative images of immunofluorescence staining for SH3GLB1 (green) and mitochondria (red) or lysosomes (red) in BMDMs. Scale bar, 20 μm. Representative (B and F) western blot and (C-E and G-I) quantification of mitophagy-related protein levels in BMDMs treated with CCCP. (J) mKeima expressed in BMDMs was imaged by confocal microscopy (mKeima-561 nm: red; mKeima-488 nm: green; scale bar, 20 μm); (K) the 561/488 nm ratio of mKeima was statistically quantified (n=3). (L) Representative flow cytometry analysis of mKeima in BMDMs. The data are presented as the means ± SEMs; P<0.05 was considered to indicate statistical significance. SH3GLB1, SH3 domain-containing GRB2-like protein B1; BMDMs, bone marrow-derived macrophages; CCCP, carbonyl cyanide-chlorophenylhydrazone.

contrast, the restoration of SH3GLB1 expression provoked ALI. Mechanistically, SH3GLB1 interacted with Rab7 to contribute to adverse mitophagy, which resulted in mitochondrial dysfunction. These findings suggested that SH3GLB1 may be a potential target for protection of the lungs against ALI induced by LPS or drowning stimuli.

ALI is characterized by infiltration of a large number of inflammatory cells, epithelial injury, pulmonary oedema, increased microvascular permeability and diffuse alveolar damage (29). Similarly, the present study found that drowning-ALI was characterized by leukocyte accumulation, pulmonary oedema, increased alveolar permeability and diffuse alveolar damage. In particular, macrophages are implicated in the inflammatory process in ALI (30). The present study performed single-cell profiling of lung immune cells isolated from drowning-ALI lungs. This demonstrated neutrophil infiltration in the early stage of acute lung injury. As the inflammation progressed, the neutrophils died and the number of recruited macrophages increased. Over time, the recruited macrophages became exhausted and tissue-resident macrophages became involved. This process is similar to that of LPS-ALI. The results of the present study indicated that macrophages were involved in the inflammatory process of drowning-ALI.

Mitochondrial quality control modulates cell fate and homeostasis and diminished mitochondrial quality control results in mitochondrial dysfunction, increased ROS production, reduced ATP production and often the induction of intrinsic apoptosis (31). A study showed that aberrant mitochondria contribute to ALI (32). The present study showed that mitochondrial injury was implicated in drowning-ALI. It focused on the mitochondrial protein SH3GLB1, a member of the endophilin protein family (33), which is located in the outer mitochondrial membrane (34). A previous study reported that SH3GLB1 plays a key role in regulating mitochondrial injury and cell death (14). The present study found that SH3GLB1 was highly expressed in macrophages, which is consistent with the pattern of macrophages in drowning-ALI. Notably, macrophages with high SH3GLB1 expression were associated with inflammation and the response to oxidative stress. The present study found that SH3GLB1 deletion protected against mitochondrial injury and oxidative stress induced by drowning or LPS. By contrast, restoring SH3GLB1 expression in the lungs provoked drowning- or LPS-induced mitochondrial dysfunction. These findings suggested for the first time that the mitochondrial protein SH3GLB1 participates in ALI.

To explore the mechanisms by which SH3GLB1 affects mitochondria, the present study found that SH3GLB1 interacted with Rab7, a small G protein of the Rab family that is located primarily in late endosomes and lysosomes (35). Rab7 plays a significant role in various inflammatory responses, particularly in regulating intracellular transport and lysosomal function (36,37). Its functions in colitis, acute pancreatitis and immune responses indicate that the regulation of Rab7 is crucial for maintaining intracellular homeostasis and alleviating inflammatory responses (38). The present study reported that SH3GLB1 provoked inflammation by the regulation of Rab7 in ALI. It has also been reported that Rab7 regulates transport from late endosomes to lysosomes and is involved in the biogenesis and degradation processes of lysosomes (39,40). Autophagy is an important form of lysosomal degradation (41). Among these processes, mitophagy plays a significant role in inflammation through lysosomal degradation (42). A previous study showed that autophagy-related key genes (including SH3GLB1) with diagnostic and prognostic value in sepsis and discovered associations between key genes and immune cell signatures (43). Sepsis induced ALI is a leading cause of poor prognosis in clinical patients (44). The present study indicated that the overexpression of SH3GLB1 led to the formation of autophagosomes, which colocalized with mitochondria and lysosomes, indicating that SH3GLB1 was involved in mitophagy. The results of the present study revealed that increased SH3GLB1 promoted mitophagy, whereas reduced SH3GLB1 inhibited mitophagy. This is similar to a study by Takahashi *et al* (14). This may provide new directions for the discovery of promising biomarkers for different factors induced ALI.

Although the findings of the present study possess some clinical relevance, there are several limitations. First, ALI-induced damage, including apoptosis, has not been extensively explored. Second, while the present study found that SH3GLB1 interacted with Rab7, it did not focus on further mechanisms. Therefore, these limitations should be considered in future studies.

In summary, the findings of the present study showed that the regulation of macrophages in drowning-ALI was similar to that in LPS-ALI. Specifically, SH3GLB1 was found to be related to macrophage inflammation and mitochondrial homeostasis. Mechanistically, SH3GLB1 was required for mitophagy regulated by Rab7. These findings suggest that SH3GLB1 may be a potential target for the protection of lungs against ALI induce by LPS or drowning stimuli.

Acknowledgements

Not applicable.

Funding

The present study was financially supported by the Program for National Science Funds of China (grant no. 82270084).

Availability of data and materials

The data generated in the present study may be requested from the corresponding author.

Authors' contributions

HJN, JYD and FGJ conceived and designed the research; HJN, JYD and YHG, WZ, JC, XG performed the experiments, analyzed the data, interpreted the results of the experiments and prepared the figures; HJN, JYD and FGJ drafted the manuscript; all the authors contributed to editing and revision. FGJ and HJN confirm the authenticity of all the raw data. All authors read and approved the final manuscript.

Ethics approval and consent to participate

All animal procedures followed the eighth edition (2011) of the Guide for the Care and Use of Laboratory Animals (https://www.ncbi.nlm.nih.gov/books/NBK54050/) and were

approved by the Fourth Military Medical University Animal Ethics Committee (approval no. 20250088).

Patient consent for publication

Not applicable.

Competing interests

The authors declare that they have no competing interests.

References

1. Jin F and Li C: Seawater-drowning-induced acute lung injury: From molecular mechanisms to potential treatments. Exp Ther Med 13: 2591-2598, 2017.
2. Qiu YB, Wan BB, Liu G, Wu YX, Chen D, Lu MD, Chen JL, Yu RQ, Chen DZ and Pang QF: Nrf2 protects against seawater drowning-induced acute lung injury via inhibiting ferroptosis. Respir Res 21: 232, 2020.
3. Sun XQ, Wu C, Qiu YB, Wu YX, Chen JL, Huang JF, Chen D and Pang QF: Heme oxygenase-1 attenuates seawater drowning-induced acute lung injury through a reduction in inflammation and oxidative stress. Int Immunopharmacol 74: 105634, 2019.
4. Zhang L, Kong D, Huang J, Wang Q and Shao L: The therapeutic effect and the possible mechanism of C-phycocyanin in lipopolysaccharide and seawater-induced acute lung injury. Drug Des Devel Ther 16: 1025-1040, 2022.
5. Jiang W, Ma C, Bai J and Du X: Macrophage SAMSN1 protects against sepsis-induced acute lung injury in mice. Redox Biol 56: 102432, 2022.
6. Jiang L, Yang D, Zhang Z, Xu L, Jiang Q, Tong Y and Zheng L: Elucidating the role of Rhodiola rosea L. in sepsis-induced acute lung injury via network pharmacology: Emphasis on inflammatory response, oxidative stress, and the PI3K-AKT pathway. Pharm Biol 62: 272-284, 2024.
7. Hsieh PC, Wu YK, Yang MC, Su WL, Kuo CY and Lan CC: Deciphering the role of damage-associated molecular patterns and inflammatory responses in acute lung injury. Life Sci 305: 120782, 2022.
8. Jiang J, Huang K, Xu S, Garcia JGN, Wang C and Cai H: Targeting NOX4 alleviates sepsis-induced acute lung injury via attenuation of redox-sensitive activation of CaMKII/ERK1/2/MLCK and endothelial cell barrier dysfunction. Redox Biol 36: 101638, 2020.
9. Zhang M, Yan X, Liu W, Sun R, Xie Y and Jin F: Endothelial semaphorin 7A promotes seawater aspiration-induced acute lung injury through plexin C1 and β1 integrin. Mol Med Rep 16: 4215-4221, 2017.
10. Li PC, Wang BR, Li CC, Lu X, Qian WS, Li YJ, Jin FG and Mu DG: Seawater inhalation induces acute lung injury via ROS generation and the endoplasmic reticulum stress pathway. Int J Mol Med 41: 2505-2516, 2018.
11. Cao Z, Lis R, Ginsberg M, Chavez D, Shido K, Rabbany SY, Fong GH, Sakmar TP, Rafii S and Ding BS: Targeting of the pulmonary capillary vascular niche promotes lung alveolar repair and ameliorates fibrosis. Nat Med 22: 154-162, 2016.
12. Cheng P, Li S and Chen H: Macrophages in lung injury, repair, and fibrosis. Cells 10: 436, 2021.
13. Cuddeback SM, Yamaguchi H, Komatsu K, Miyashita T, Yamada M, Wu C, Singh S and Wang HG: Molecular cloning and characterization of Bif-1. A novel Src homology 3 domain-containing protein that associates with Bax. J Biol Chem 276: 20559-20565, 2001.
14. Takahashi Y, Hori T, Cooper TK, Liao J, Desai N, Serfass JM, Young MM, Park S, Izu Y and Wang HG: Bif-1 haploinsufficiency promotes chromosomal instability and accelerates Myc-driven lymphomagenesis via suppression of mitophagy. Blood 121: 1622-1632, 2013.
15. Takahashi Y, Karbowski M, Yamaguchi H, Kazi A, Wu J, Sebti SM, Youle RJ and Wang HG: Loss of Bif-1 suppresses Bax/Bak conformational change and mitochondrial apoptosis. Mol Cell Biol 25: 9369-9382, 2005.
16. Wong AS, Lee RH, Cheung AY, Yeung PK, Chung SK, Cheung ZH and Ip NY: Cdk5-mediated phosphorylation of endophilin B1 is required for induced autophagy in models of Parkinson's disease. Nat Cell Biol 13: 568-579, 2011.
17. Wang DB, Kinoshita Y, Kinoshita C, Uo T, Sopher BL, Cudaback E, Keene CD, Bilousova T, Gylys K, Case A, *et al*: Loss of endophilin-B1 exacerbates Alzheimer's disease pathology. Brain 138(Pt 7): 2005-2019, 2015.
18. Wang DB, Uo T, Kinoshita C, Sopher BL, Lee RJ, Murphy SP, Kinoshita Y, Garden GA, Wang HG and Morrison RS: Bax interacting factor-1 promotes survival and mitochondrial elongation in neurons. J Neurosci 34: 2674-2683, 2014.
19. Zhou M, Meng L, He Q, Ren C and Li C: Valsartan attenuates LPS-induced ALI by modulating NF-κB and MAPK pathways. Front Pharmacol 15: 1321095, 2024.
20. Ma L, Chen X, Wang R, Duan H, Wang L, Liang L, Nan Y, Liu X, Liu A and Jin F: 3,5,4'-Tri-O-acetylresveratrol decreases seawater inhalation-induced acute lung injury by interfering with the NF-κB and i-NOS pathways. Int J Mol Med 37: 165-172, 2016.
21. McGuigan RM, Mullenix P, Norlund LL, Ward D, Walts M and Azarow K: Acute lung injury using oleic acid in the laboratory rat: Establishment of a working model and evidence against free radicals in the acute phase. Curr Surg 60: 412-417, 2003.
22. Deng J, Chang X, Zhang X, Li C, Guo G, Song H, Zheng Y, Zhang C, Yang B, Zhang C, *et al*: Endophilin B1 is essential for maintaining cardiac function by regulating mitocytosis. Cell Mol Life Sci 82: 130, 2025.
23. Yan J, Zhang Y, Yu H, Zong Y, Wang D, Zheng J, Jin L, Yu X, Liu C, Zhang Y, *et al*: GPSM1 impairs metabolic homeostasis by controlling a pro-inflammatory pathway in macrophages. Nat Commun 13: 7260, 2022.
24. Engels M, Bilgic E, Pinto A, Vasquez E, Wollschläger L, Steinbrenner H, Kellermann K, Akhyari P, Lichtenberg A and Boeken U: A cardiopulmonary bypass with deep hypothermic circulatory arrest rat model for the investigation of the systemic inflammation response and induced organ damage. J Inflamm (Lond) 11: 26, 2014.
25. Yang R, Ruan B, Wang R, Zhang X, Xing P, Li C, Zhang Y, Chang X, Song H, Zhang S, *et al*: Cardiomyocyte βII spectrin plays a critical role in maintaining cardiac function by regulating mitochondrial respiratory function. Cardiovasc Res 120: 1312-1326, 2024.
26. Deng J, Zhang N, Chen F, Yang C, Ning H, Xiao C, Sun K, Liu Y, Yang M, Hu T, *et al*: Irisin ameliorates high glucose-induced cardiomyocytes injury via AMPK/mTOR signal pathway. Cell Biol Int 44: 2315-2325, 2020.
27. Qi B, He L, Zhao Y, Zhang L, He Y, Li J, Li C, Zhang B, Huang Q, Xing J, *et al*: Akap1 deficiency exacerbates diabetic cardiomyopathy in mice by NDUFS1-mediated mitochondrial dysfunction and apoptosis. Diabetologia 63: 1072-1087, 2020.
28. Deng Z, He M, Hu H, Zhang W, Zhang Y, Ge Y, Ma T, Wu J, Li L, Sun M, *et al*: Melatonin attenuates sepsis-induced acute kidney injury by promoting mitophagy through SIRT3-mediated TFAM deacetylation. Autophagy 20: 151-165, 2024.
29. Xia L, Zhang C, Lv N, Liang Z, Ma T, Cheng H, Xia Y and Shi L: AdMSC-derived exosomes alleviate acute lung injury via transferring mitochondrial component to improve homeostasis of alveolar macrophages. Theranostics 12: 2928-2947, 2022.
30. Fan EKY and Fan J: Regulation of alveolar macrophage death in acute lung inflammation. Respir Res 19: 50, 2018.
31. Larson-Casey JL, He C and Carter AB: Mitochondrial quality control in pulmonary fibrosis. Redox Biol 33: 101426, 2020.
32. Islam MN, Das SR, Emin MT, Wei M, Sun L, Westphalen K, Rowlands DJ, Quadri SK, Bhattacharya S and Bhattacharya J: Mitochondrial transfer from bone-marrow-derived stromal cells to pulmonary alveoli protects against acute lung injury. Nat Med 18: 759-765, 2012.
33. Sparks AB, Hoffman NG, McConnell SJ, Fowlkes DM and Kay BK: Cloning of ligand targets: Systematic isolation of SH3 domain-containing proteins. Nat Biotechnol 14: 741-744, 1996.
34. Li J, Barylko B, Eichorst JP, Mueller JD, Albanesi JP and Chen Y: Association of endophilin B1 with cytoplasmic vesicles. Biophys J 111: 565-576, 2016.
35. Rodriguez-Furlan C, Borna R and Betz O: RAB7 GTPases as coordinators of plant endomembrane traffic. Front Plant Sci 14: 1240973, 2023.
36. Bucci C, Bakke O and Progida C: Rab7b and receptors trafficking. Commun Integr Biol 3: 401-404, 2010.
37. Mousa SA, Shaqura M, Khalefa BI, Zöllner C, Schaad L, Schneider J, Shippenberg TS, Richter JF, Hellweg R, Shakibaei M and Schäfer M: Rab7 silencing prevents μ-opioid receptor lysosomal targeting and rescues opioid responsiveness to strengthen diabetic neuropathic pain therapy. Diabetes 62: 1308-1319, 2013.

38. Kelly C, Canning P, Buchanan PJ, Williams MT, Brown V, Gruenert DC, Elborn JS, Ennis M and Schock BC: Toll-like receptor 4 is not targeted to the lysosome in cystic fibrosis airway epithelial cells. Am J Physiol Lung Cell Mol Physiol 304: L371-L382, 2013.
39. Schleinitz A, Pöttgen LA, Keren-Kaplan T, Pu J, Saftig P, Bonifacino JS, Haas A and Jeschke A: Consecutive functions of small GTPases guide HOPS-mediated tethering of late endosomes and lysosomes. Cell Rep 42: 111969, 2023.
40. Jin X, Wang K, Wang L, Liu W, Zhang C, Qiu Y, Liu W, Zhang H, Zhang D, Yang Z, *et al*: RAB7 activity is required for the regulation of mitophagy in oocyte meiosis and oocyte quality control during ovarian aging. Autophagy 18: 643-660, 2022.
41. Levine B and Kroemer G: Biological functions of autophagy genes: A disease perspective. Cell 176: 11-42, 2019.
42. Picca A, Faitg J, Auwerx J, Ferrucci L and D'Amico D: Mitophagy in human health, ageing and disease. Nat Metab 5: 2047-2061, 2023.
43. Yang L, Zhou L, Li F, Chen X, Li T, Zou Z, Zhi Y and He Z: Diagnostic and prognostic value of autophagy-related key genes in sepsis and potential correlation with immune cell signatures. Front Cell Dev Biol 11: 1218379, 2023.
44. Wu D, Spencer CB, Ortoga L, Zhang H and Miao C: Histone lactylation-regulated METTL3 promotes ferroptosis via m6A-modification on ACSL4 in sepsis-associated lung injury. Redox Biol 74: 103194, 2024.